HTS CroCo - a Strand for High Direct Current Applications

HTS CroCo - a Strand for High Direct Current Applications

M J Wolf, W H Fietz, M Heiduk, R Heller, C Lange, A Preuß, and K-P Weiss

Karlsruhe Institute of Technology, Institute for Technical Physics, Hermann-von-Helmholtz-Platz 1, 76344 Eggenstein-Leopoldshafen, Germany

michael.wolf@kit.edu

Abstract. High temperature superconductors (HTS) are discussed as energy-efficient solutions for applications needing high direct currents beyond 10 kA e.g. for large high-field magnets or bus bar systems in industrial electrolysis plants. A number of high-current cable concepts based on REBCO tapes were developed such as the Roebel cable, co-axially wound tapes and several stacked-tape arrangements, among them the HTS CrossConductor (HTS CroCo), a stacked-tape conductor with high current density developed at KIT. In this manuscript, the experimental test of a high DC demonstrator, termed Supra-DC-Cable, made from twelve HTS CroCo strands is presented. The demonstrator was tested successfully at T = 77 K, reaching the expected critical current of 33 kA at 77 K and even for a constant-current operation at 36 kA for more than 30 minutes limited by the copper connections, not the superconducting cable. Currents and voltages were measured in all twelve strands individually during the parallel operation in the cable. These measured data allow the experimental validation of the modelled current distribution, based on the individual characterization of the twelve strands.

1. Introduction to High Direct Current Applications

Global warming is one of today's key challenges and technologies to decarbonize and to increase the energy-efficiency of all aspects of our way of living are of key interest. Within the German "energy transition" it is targeted to reduce the primary energy consumption by 20 % in 2020 and 50 % by 2050 compared to the 2008 values [1]. The replacement of carbon-based fuels by renewable energy sources are one major aspect. About 47% of Germany's net electric power is consumed by industry [2] and nearly half of this value by the so-called energy-intensive industries [3]. Consequently, improvements in the energy efficiency of these industries can provide a big contribution to the reduction goals.

The reduction of electric losses by superconducting cables, in particular based on high temperature superconductors (HTS), can be one technology to improve energy efficiency. As $P_{loss} = R\,I^2$, high current applications can benefit in particular from superconducting cable systems, where in the cable the resistance is $R \approx 0$. Highest currents are encountered in aluminum electrolysis, where currents can reach up to 600 kA [4], [5] other electrolysis processes e.g. for magnesium or chlorine use currents in the ten to several hundred kilo ampere range [4-7]. Most of these applications operate almost continuously at high loads and allow therefore for substantial energy savings. HTS can provide substantially higher current densities than conventional copper or aluminum systems and can reduce size and weight of installations or allow for more powerful systems in existing ducts (retrofitting) [8]. Electrolysis may be one important field of application for superconducting high DC systems but there are several other potential applications where energy-efficiency can be improved or new concepts can be enabled.

In railway systems, superconducting DC cables are discussed as solution to allow for lower voltage drop along the lines and reduced number of converters [9]. In large data centers, low-voltage DC bus systems could be realized by superconducting systems reducing space, weight or allow for facility-wide

installations at 48 V_{DC} or 400 V_{DC} [5], [10]. Potential new applications include DC grids on large ships [5] or in future electric airplanes [11], [12].

Over the last years, several DC cable systems with currents of 10 kA and more were realized. These include two 20 m long 20 kA test cables of Magnesium-diboride based bus bar system to power accelerator magnets at CERN [13], a 360-meter-long 10 kA system for an aluminum plant in China [14] and a 25-meter-long 20 kA system for a Chlorine electrolysis in Germany [7].

At KIT, a small-scale test setup was set up to test high-current cable prototypes of about 4 meters length in an liquid nitrogen bath operated at ambient pressure, i.e. T = 77 K, at currents up to 50 kA. The first tested cable was a cable consisting of twelve so-called HTS CroCo strands with target critical current of about 35 kA, termed Supra-DC-Cable. This prototype cable was realized in order to test recently developed design and calculation codes for high DC cable systems [15] and the fabrication of the required amount of HTS CroCo strands. Details can be found in [15], [16] and [17].

2. The Supra-DC-Cable Test Setup

The Supra-DC-Cable demonstrator test setup is shown in Figure 1. It consists of twelve HTS CroCo strands which are arranged in a circular arrangement on a central carrier of 110 mm diameter, as depicted in Figure 1(b). Details of the design was described in previous work [17]. Each individual HTS CroCo strand consists of a series connection of the central superconducting part soldered at each end to a copper cylinder (CC) over a length of 100 mm. The copper cylinders are soldered to Copper litz wires (CL) of 300 mm² cross-section. Finally, the copper litz wires are soldered to Cable shoes (CS) which are used to connect the wires to common terminals in the LN_2 bath. The voltage drops over all soldered connections and the litz wires were recorded. The voltage tap configuration is depicted in Figure 2. Details on the current source and data acquisition system were reported in [17]. The long CL wires serve several purposes: First, they allow for a compensation of thermal contraction, second, they provide the required flexibility during the mounting of the twelve strands in the bath, and third, their electric resistance allows to determine the current flowing in the individual HTS CroCo strands by measuring the voltage drop in the parallel connection of the Supra-DC-Cable demonstrator setup. Using the resistivity of copper of $\rho \sim 2$ nΩm at T = 77 K [18], one expects a resistance of 3 μΩ over a length of 450 mm at a cross-section of 300 mm².

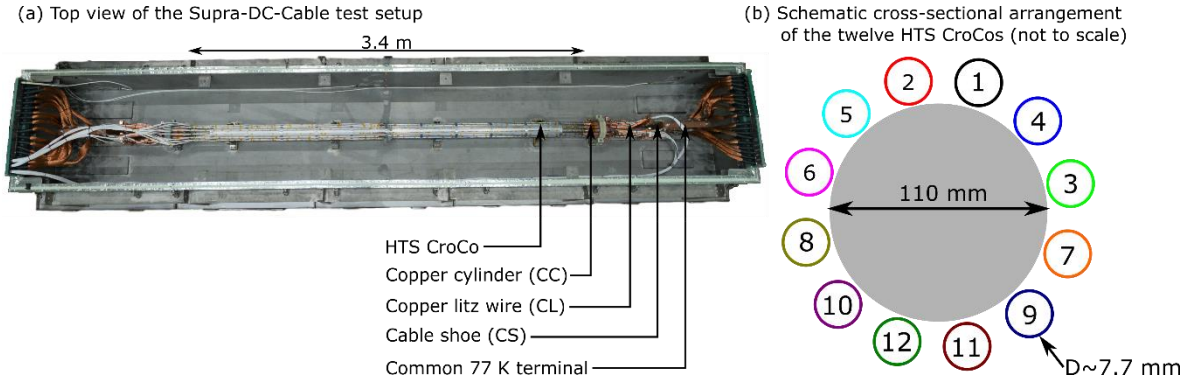

Figure 1: (a) Open cryostat with Supra-DC-Cable demonstrator installed. The total length of the cryostat is 6 meters. The components of each of the twelve strands are labelled.
(b) Schematics (not to scale) of the concentric arrangement of the twelve HTS CroCo strands together with the position of each strand in the demonstrator. Note that the colours of the CroCos correspond to colours of the symbols in the graphs.

3. Improvements after initial test campaigns

In previous work [16], all twelve strands were characterized individually in a LN_2 bath prior to the first Supra-DC-Cable test campaign. The characterization included the individual measurement of the strands' critical currents and n-values at $T = 77$ K, self-field and the lead resistances in the configuration shown in Figure 2(a) and were already published in [16] and [17]. Critical currents range between 2.89 kA (CroCo # 11) and 3.68 kA (CroCo # 5) due to a combination of different tape performance and improvements in HTS CroCo manufacturing in the course of this project. During the analysis of these measurements, a significantly higher lead resistance was observed on HTS CroCo strand # 6, which could not be straight-forwardly explained. Therefore, this single-strand measurement of HTS CroCo #6 was repeated and cross-checked resulting in resistance values much closer to results obtained in the other eleven strands. The most likely reason for the deviation in the initial measurement of CroCo # 6 is a not complete thermalization of one cable end which led to higher lead resistances there. Figure 2(b) displays a stacked plot of the resistances of the individual parts of the cable for all twelve HTS CroCo strands. It can be seen that the total lead resistance ranges between 7.8 μΩ and 8.9 μΩ, i.e. differing by less than 15% between the highest and lowest value. Moreover, the contribution from the copper litz wire is the dominant part on each side, contributing to about 3 μΩ each. The connection to the HTS CroCo is ranging between 150 nΩ and 320 nΩ, and is therefore by at least an order of magnitude smaller than the contribution from the copper litz wire.

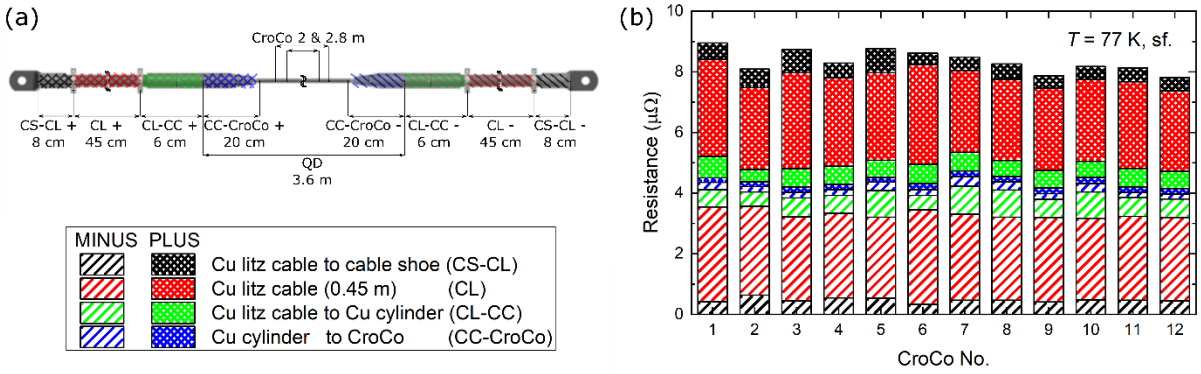

Figure 2: (a) Schematics of the components of the leads connecting each HTS CroCo strand. Note that checkered coloring is used for the plus pole, striped coloring is used for the minus pole.
(b) Measured resistance values of the individual parts of the leads connecting each HTS CroCo strand at $T = 77$ K.

In the parallel connection of the twelve HTS CroCos and their individual leads, the voltage in each one must be the same, which allows to calculate the individual HTS CroCo currents I_i and the cable current I_{cable} for a given voltage from the equations

$$V(I_{cable}) = V_{lead},i + V_{HTS,i} = R_{lead,i}\, I_i + E_c L \left(\frac{I_i}{I_{c,i}}\right)^{n_i}, \text{where} \quad (1)$$

$$R_{lead,i} = R_i^{CS-CL,+} + R_i^{CL,+} + R_i^{CL-CC,+} + R_i^{CC-CroCo,+} + R_i^{CC-CroCo,-} + R_i^{CL-CC,-} + R_i^{CL,-} + R_i^{CS-CL,-}$$

$$\text{and } I_{cable} = \sum_{i=1}^{12} I_i$$

The only unknown resistance contribution which could not be checked in previous characterization is the resistance of the clamped cable shoe to the common copper termination block (see Figures 1 and 2(a)). In an earlier test campaign of the Supra-DC-Cable [17], a weak connection on one strand led to

an unequal current distribution. This issue was eliminated in this test campaign by using bolts with the same thermal expansion coefficient as copper for the connection of the cable shoes.

4. Performance of the Supra-DC-Cable at constant current ramp rate

The cable current was increased at a constant current ramp rate of 500 A/s until it was stopped by the quench detection system at ~ 40 kA. Figure 3 shows the electric field as calculated from the voltage measured between the voltage taps of 2.8 m separation. It is shown on a logarithmic scale in all twelve HTS CroCo strands as a function of the total cable current in the range from 20 kA to 42 kA. The symbols denote the measured electric field values, the dashed lines denote calculated values according to Equation 1 from the parameters of the individual strand characterization. It should be noted that there are no free fitting parameters in the model.

The critical electric field $E_c = 1\mu V/cm$ is reached first in HTS CroCo # 12 at a total cable current of ~ 33 kA, followed about 2 kA later by strand # 11. At 37.5 kA, CroCo # 2 reaches the critical electric field. The other strands follow, but not all reach E_c until the end of the measurement. These observations can be very well understood from the model described above, because the resistance of the Cu-litz of the individual CroCos decouple the transition from superconductivity to resistive behavior for the individual CroCos. At a substantial non-zero electric field, the transition to the normal state is very well matched by the model. At currents below 30 kA, a small, but non-zero voltage is seen in the measured data but not in the model.

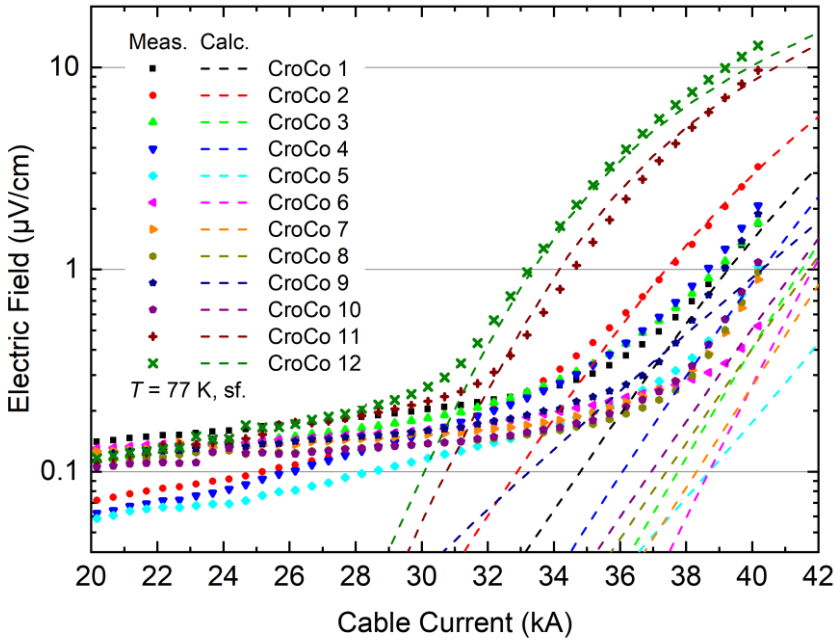

Figure 3: Electric field on a logarithmic scale in all twelve HTS CroCo strands as a function of the total cable current in the range from 20 kA to 42 kA. The symbols denote the measured electric field values, dashed lines denote calculated values according to Equation 1 without free fitting parameters.

In order to gain further insight into the current and voltage distributions during the current ramp, the currents of the individual HTS CroCo strands are calculated from the voltage drop over the copper litz cable at the positive and negative pole, $V_i^{CL,+}$ and $V_i^{CL,-}$, with the known resistances of the cable $R_i^{CL,+}$ and $R_i^{CL,-}$ (Figure 4). Then the mean value of the plus and minus pole, $I_i = \frac{1}{2}\left(\frac{V_i^{CL,+}}{R_i^{CL,+}} + \frac{V_i^{CL,-}}{R_i^{CL,-}}\right)$ and the

standard deviation $\sigma_{I_i} = \sqrt{\left(\frac{V_i^{CL,+}}{R_i^{CL,+}} - I_i\right)^2 + \left(\frac{V_i^{CL,-}}{R_i^{CL,-}} - I_i\right)^2}$ are calculated. In order to check for consistency, all currents in the individual CroCos are added and compared to the total cable current obtained from a separate measurement (described in detail in [17]). Over most of the current range, the sum of the individual currents is about 2% to 3% larger than the total cable current but in agreement when the uncertainty of the sum of the individual CroCo currents is also considered as it can be seen from Figure 4.

For further analysis, the individual CroCo currents are therefore normalized to the total cable current by considering $I_{i,corr}(I_{cable}) = \frac{I_i}{\sum_1^{12} I_i} I_{cable}$.

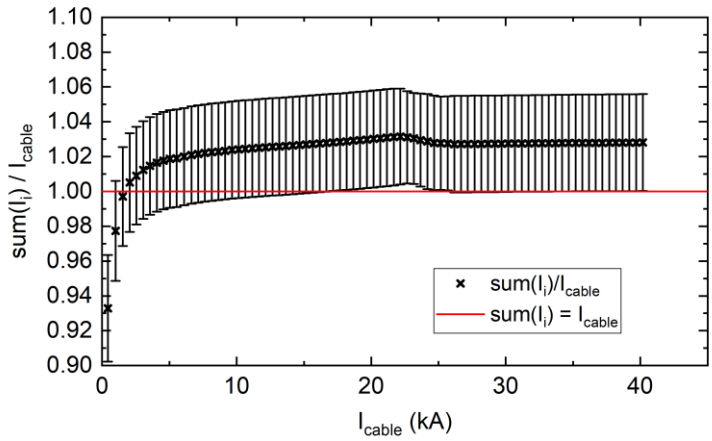

Figure 4: Sum of the individual HTS CroCo currents and uncertainties as obtained from the voltage drop in the copper litz wires and the previously measured resistances normalized to the total cable current. The red line indicates an ideal agreement $\sum_1^{12} I_i / I_{cable} = 1$.

This measured and corrected CroCo cable current is then calculated and plotted in Figure 5 as a function of the total cable current in the range from 30 kA to 41 kA for CroCos 1, 9, and 12 (filled symbols). This selection of strands is chosen as CroCo 1 has the highest overall lead resistance, CroCo 9 the second lowest lead resistance and second highest critical current and CroCos 12 has the second smallest critical current and lowest lead resistance of the twelve strands. The remaining nine strands are not shown to improve the clarity.

In addition, the expected individual CroCo currents according to Equation (1) from the single strand characterization are presented as dashed lines. The colors correspond to those of the symbols of the CroCo strands. A very good agreement between the measured individual strand critical currents and the expectation from the calculations is observed. In particular, CroCo 9 shows the highest strand current as expected from the comparatively low lead resistance. Even at the highest cable current, the strand's critical current is not reached. For CroCo 1, the situation is reversed: Due to the highest lead resistance, it carries the lowest current. CroCo12 is of particular interest as at a cable current of ~33 kA, the critical current of of 2.93 kA is reached. At higher currents, the slope of the strand current starts to decrease until a leveling off at highest currents of ~ 40 kA is almost observed. This behavior is expected as the total voltage over the twelve CroCos in parallel connection is expected to be the same and since at $I_i > I_{c,i}$ the superconducting cable part starts to develop a substantial voltage in the millivolt range (see Figure 3) in addition to the voltage drop over the leads of ~ 25 mV at a strand current of ~ 3 kA, therefore the slope of the individual current as function of the total cable current decreases.

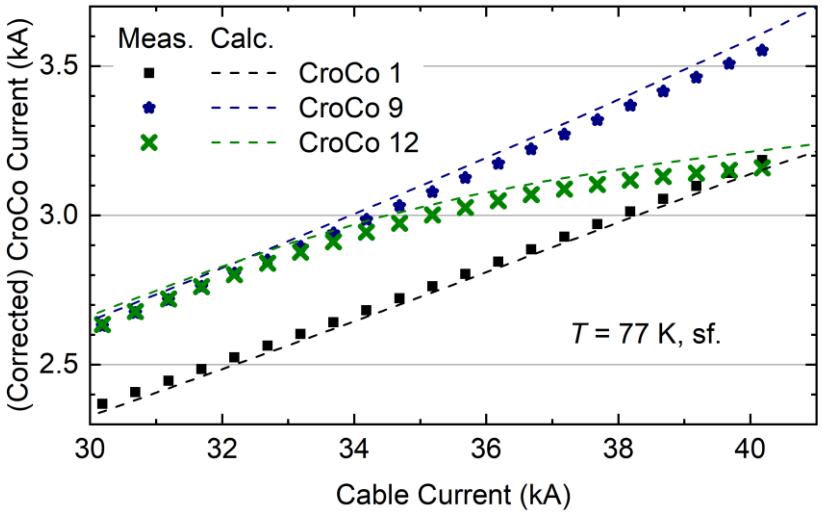

Figure 5: Current in HTS CroCos #1, #9 and #12 as function of the Cable current. The measured and corrected HTS CroCo current is shown by filled symbols, the expectation from modelling based on individual-strand characterization is given by dashed lines. The colours of the symbols and lines correspond to the CroCos as indicated in Figure 1.

5. Influence of cable current ramp rates on electric field evolution in the HTS CroCos

By a series of cable current sweeps it was investigated how the transition to normal conducting state changes. Figure 6 shows the electric field on HTS CroCo #12, i.e. the strand which showed the highest electric field of all twelve strands, as function of the cable current for current ramp rates from 25 A/s to 2500 A/s. It can be seen that for current ramp rates smaller than 500 A/s, lower maximum cable currents were achieved. This behavior is attributed to insufficient cooling at the electric fields beyond 10 µV/cm. The substantially longer measurement time corresponding to smaller ramp rates leads to thermal runaway and a steepening of the transition to normal state.

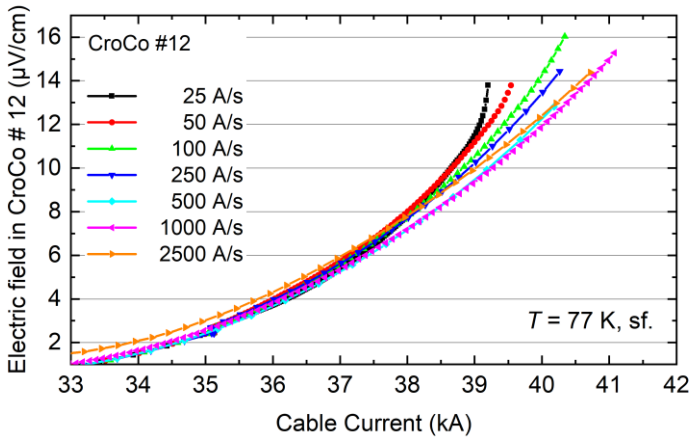

Figure 6: Electric field in CroCo # 12 at cable currents > 33 kA for different ramp rates.

6. Steady-state operation

In a final series of measurements, the limit of stable cable operation was investigated. Therefore, the cable current was kept constant at a target value and until either thermal runaway was observed and the

quench detection system triggered a current shutdown or until an over-temperature on the room temperature bus bar system was observed. Figure 7 shows the electric field on HTS CroCo #12 as function of the time since the target current was reached for various currents.

The series of measurements was started at 36 kA, where the electric field in CroCo #12 already exceeded the critical electric field by a factor of 4. Still, cable operation was possible for more than 39 minutes, before the current had to be shut down due to over-temperature of the room-temperature bus bar. For the same reason, operation at 37 kA had to be stopped after 11 minutes where still no thermal runaway was detected. Yet a continuous small increase of the electric field is observed. At 37.5 kA, thermal runaway triggered the quench detection system after ~2.5 minutes. With increasing current, the thermal runaway occurred after shorter time until at 39.5 kA it started right after the target current was reached and no stable operation was observed.

It should be noted that at these current levels, about 500 W of Joule heating from the resistance of each lead is generated on each pole which adds to the heat generated in the outer leads connecting the room temperature end of the common 77 K termination in Figure 1 to room temperature. This heat leads to evaporation of liquid nitrogen and additional turbulence in the cryostat. In a real cable system, e.g. cooled by a flow of sub-cooled liquid nitrogen, such large heat intake is of course prohibitive.

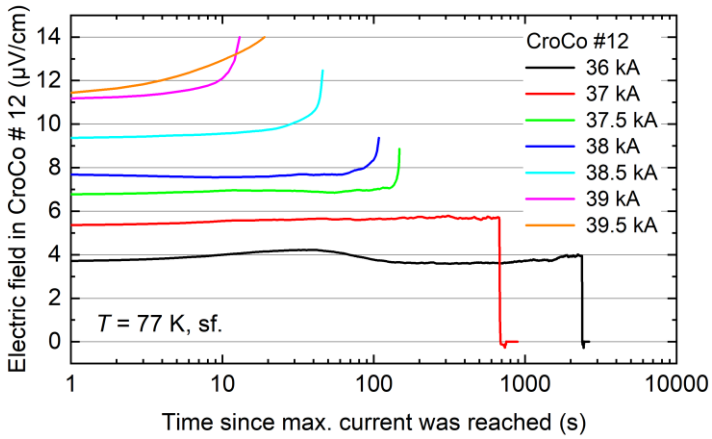

Figure 7: Electric field in CroCo # 12 as function of time for different cable currents.

7. Outlook and further work

During this test campaign, all HTS CroCo strands were connected through the ~ 4 µΩ large lead resistances per pole to the common termination block. The total voltage at the highest current of 40 kA was consequently dominated by the voltage drop over the lead resistances even for the CroCo strands which exceeded E_c there, e.g. CroCo #12. Figure 8(a) shows the calculated voltage distribution between the superconducting and the lead part in detail. The large series resistance therefore prevents effective current sharing between the strands connected in parallel.

One option to improve current sharing between the HTS CroCo strands is to add a common connector after the copper litz wires such that the only (unavoidable) series resistance is the resistance of the soldered connection between the common connector to the superconducting HTS CroCo strand. If one assumes this resistance of equal the average of the CC-CroCo resistance of ~200 µΩ (see Figure 2 (b)), and the resistance within the common connector to be negligible, the voltage distribution between lead and HTS CroCos and within HTS CroCos is now much more equalized as it can be seen from the calculation shown in Figure 8(b). The realization of the common connector and the test in modified arrangement will be discussed in further work.

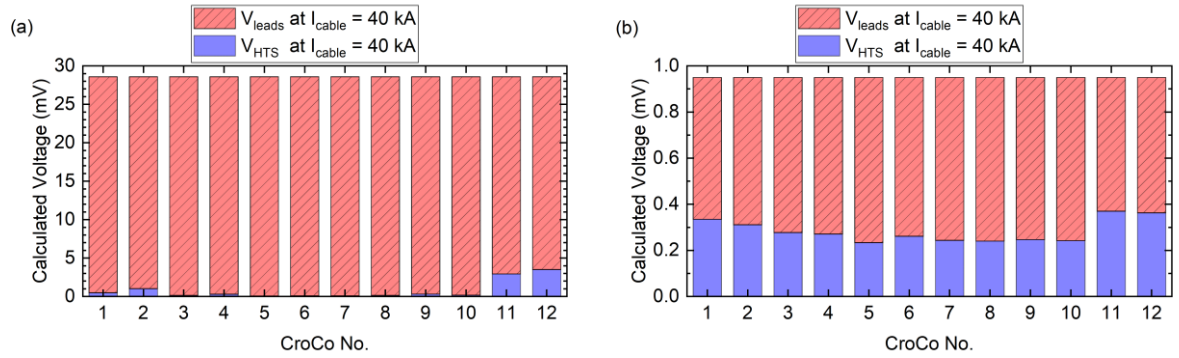

Figure 8: Calculated voltage distributions between leads (red, shaded) and HTS CroCo (blue) at a cable current of 40 kA. (a) Supra-DC-Cable connected "as-is", (b) with additional common connector to which the HTS CroCos are soldered directly assuming an equal solder resistance of 200 nΩ each. Note the different scale of the voltage axis.

8. Summary

In this manuscript, results on the Supra-DC-Cable demonstrator consisting of twelve superconducting HTS CroCo strands are discussed. In the design of the demonstrator, each HTS CroCo strand was connected by individual copper litz wire which could be used to determine the currents flowing in the individual strands. The critical electric field was reached at a cable current of 33 kA in HTS CroCo strand # 12. However, due to the variation of series resistances, some of the CroCos did not reach the critical electrical field even at highest cable currents.

This measurement confirms the electric DC circuit model – in addition to the critical current also the voltage dependence is very well confirmed. At highest currents, a decrease of the slope of the strands which carried currents beyond their critical current was observed – in agreement with the model.

Additionally, the performance of the demonstrator in steady-state operation was checked and at a cable current of 36 kA, stable operation of more than 39 minutes – limited by the room-temperature connection, not by the superconductor – was observed.

In further work it is targeted to allow for current sharing by adding a common connector immediately at the HTS CroCo ends. The realization of this modified demonstrator is under way and will be reported in further work.

References

[1] Bundesministerium für Wirtschaft und Technologie (Hrsg.): Energiekonzept für eine umweltschonende, zuverlässige und bezahlbare Energieversorgung. Online: https://www.bmwi.de/Redaktion/DE/Downloads/E/energiekonzept-2010.html, last accessed: 02.12.2019.

[2] Bundesverband der Energie- und Wasserwirtschaft (bdew), „Entwicklung des Nettostromverbrauchs in Deutschland", online: https://www.bdew.de/media/documents/Nettostromverbrauch_nach_Verbrauchergruppen_Entw_10J_online_o_jaehrlich_Ki_29032019.pdf, last accessed: 02.12.2019.

[3] Die Energieintensiven Industrien in Deutschland (EID). http://www.energieintensive.de/ last accessed: 02.12.2019

[4] Kvande, H and Drablos P A 2014 The aluminum smelting process and innovative alternative technologies. In: Journal of occupational and environmental medicine *American College of Occupational and Environmental Medicine* **56** (5) Suppl. S23–32.

[5] Morandi, A 2015 HTS dc transmission and distribution: concepts, applications and benefits. *Superconductor Science and Technology* **28** (12) 123001.

[6] Friedrich, H E (Eds.), Mordike B L (Eds.) 2006 *Magnesium technology: Metallurgy, design data, applications*. Berlin, Heidelberg : Springer, ISBN 9783540205999
[7] Elschner, S Superconducting DC-Busbar for high current applications. Presented at 13th EUCAS 2017, Geneva, online: https://indico.cern.ch/event/659554/contributions/2709494/attachments/1527269/2388459/3LO4-07_Steffen_Elschner_Room_1.pdf.
[8] Michael, P C *et al.* 2015 Design and test of a prototype 20 kA HTS DC power transmission cable *IEEE Trans. Appl. Supercond.*, **25** (3) 5401005
[9] Tomita, M *et al.* 2012 Development of 10 kA high temperature superconducting power cable for railway systems. *J. Appl. Phys.* **111** (6) 063910
[10] Pratt, A *et al.* 2007 Evaluation of 400 V dc distribution in telco and data centers to improve energy efficiency, *Telecommunications Energy Conf.*, INTELEC 2007, https://doi.org/10.1109/INTLEC.2007.4448733
[11] Luongo, C A *et al.* 2009 Next generation more-electric aircraft: A potential application for HTS superconductors *IEEE Trans. Appl. Supercond.* **19** (3) 1055–1068
[12] Berg, F *et al.* 2015 HTS electrical system for a distributed propulsion aircraft *IEEE Trans. Appl. Supercond.* **25 (**3) 5202705
[13] Ballarino, A and Flükiger, R 2017 Status of MgB2 wire and cable applications in Europe. *Journal of Physics: Conference Series* **871** (1) 012098.
[14] Zhang D *et al.* 2015 Stability analysis of the cable core of a 10 kA HTS DC power cable used in the electrolytic aluminum industry *IEEE Trans. Appl. Supercond.* **25** (3) 5402304.
[15] Preuß, A Development of high temperature superconductor cables for large current applications, *KIT Scientific Publishing*, in press.
[16] Preuss, A *et al.* 2019 Production and characterization of strands for a 35 kA HTS DC cable demonstrator *IEEE Trans. Appl. Supercond.* **29** (5) 5402905
[17] Weiss K.-P. *et al.*, Development and test of a 35 kA - HTS CroCo cable demonstrator presented at EUCAS 2019 (Glasgow, UK), accepted for publication at *Journal of Physics – Conference series*.
[18] Hust, J G and Lankford, A B 1984 Thermal conductivity of aluminum, copper, iron, and tungsten for temperatures from 1 K to the melting point. *National Bureau of Standards, Boulder, CO, NBSIR* 84-3007.
[19] Bagrets, N *et al.* 2014 Low temperature thermal and thermo-mechanical properties of soft solders for superconducting applications *IEEE Trans. Appl. Supercond.* **24** (3) 7800203